International Journal of Pharmaceutics 568 (2019) 118466

Contents lists available at ScienceDirect

International Journal of Pharmaceutics

journal homepage: www.elsevier.com/locate/ijpharm

Treatment for chemical burning using liquid crystalline nanoparticles as an ophthalmic delivery system for pirfenidone

Rummenigge Oliveira Silva[a], Bruna Lopes da Costa[a], Flavia Rodrigues da Silva[a,b,*], Carolina Nunes da Silva[a], Mayara Brandão de Paiva[a], Lays Fernanda Nunes Dourado[a], Ângelo Malachias[c], Adriano Antunes de Souza Araújo[d], Paula Santos Nunes[b], Armando Silva-Cunha[a]

[a] Faculty of Pharmacy, Universidade Federal de Minas Gerais, Belo Horizonte, MG 31270-901, Brazil
[b] Graduate Program in Applied Science to Health, Universidade Federal de Sergipe, Lagarto, SE 49400-000, Brazil
[c] Department of Physics, Exact Sciences Institute, Universidade Federal de Minas Gerais, 31270-901 Belo Horizonte, Minas Gerais, Brazil
[d] Department of Pharmacy, Universidade Federal de Sergipe, SE 49100-000, Brazil

ARTICLE INFO

Keywords:
Ocular chemical burns
Pirfenidone
Liquid crystalline nanoparticles
Cornea
Wound healing

ABSTRACT

Some recent studies have shown that pirfenidone (PFD) has favorable results in the healing process of the cornea. However, PFD in solution exhibits short half-life after topical application, and in this context, a liquid crystal nanoparticle system containing PFD (PFD-LCNPs) was developed. The nanoparticles were characterized by transmission electron microscopy, atomic force microscopy, small angle X-ray diffraction and polarized light microscopy. The PFD-LCNPs had particle size and zeta potential of 247.3 nm and −33.60 mV (stores at 4 °C), respectively, and 257.5 nm and −46.00 mV (stored at 25 °C), respectively. The pH of the formulation was 6.9 and the encapsulation efficiency was 35.9%. The in vitro release profiles indicated that PFD sustained release from PFD-LCNPs for up to 12 h. In vitro study of ocular irritation (HET-CAM test) concluded that components of the formulation are well tolerated for ocular administration. Corneal re-epithelialization time after chemical burning was significantly reduced in rabbits treated with PFD-loaded LCNPs when compared to the group treated with a vehicle. In addition, the anti-inflammatory action of pirfenidone was observed by reducing myeloperoxidase activity (MPO) and inflammatory cells in the histology of the tissues of animals treated with PFD-LCNPs. These findings indicated that the PFD-LCNPs might have the potential for effective ocular drug delivery.

1. Introduction

The ocular chemical burns are responsible for 11.5% to 22.1% of ocular injuries in an ophthalmic emergency (Wagoner, 1997). Estimated the world incidence rate for chemical ocular injury represents over 350,000 new chemical ocular injury cases every year (Shanbhag et al., 2018). Chemical ocular injury is common and when severe, can lead to corneal blindness, which it has a significant impact on vision-related quality of life, and create a substantial expense for local health care systems (Wagoner, 1997, Le et al., 2011, Haring et al., 2016). Eventually, loss of visual function due to corneal neovascularization, scarring, and ulceration may ensue (Jawaheer et al., 2017). Conventional treatment focuses on the reduction of inflammation, foster re-epithelialization, avoid further epithelial and stromal breakdown, prevent infections and wound healing complications (Khan et al., 2007, Hamill et al., 2013, Baradaran-Rafii et al., 2017). Biological agents that are rich sources of growth factors have been used topically in ocular burns because it has anti-inflammatory and anti-fibrotic properties that

Abbreviations: AFM, atomic force microscope; ANOVA, analysis of variance; BCS, biopharmaceutics classification system; Blank-LCNPs, Blank nanoparticles; BS, backscattering; CMC, carboxymethylcellulose; EE %, encapsulation efficiency; HET-CAM, Hen's Egg Test-Chorioallantoic Membrane test; HPLC–UV, high performance liquid chromatography with ultraviolet detection; MO, monoolein; PLM, polarized light microscopy; MPO, myeloperoxidase; NAG, N-acetylglucosaminidase; OII, ocular irritation index; PBS, phosphate-buffered saline; PDI, polydispersity index; PFD, pirfenidone; PFD-LCNPs, liquid crystal nanoparticle system containing pirfenidone; PLGA, poly(lactic-co-glycolic acid); SAXS, small-angle X-ray scattering; SEM, standard error of the mean; STF, simulated tear fluid; TEM, transmission electron microscopy; TGF-β, transforming growth factor

* Corresponding author at: Faculty of Pharmacy, Universidade Federal de Minas Gerais, Belo Horizonte, MG 31270-901, Brazil.
E-mail address: armando@farmacia.ufmg.br (F.R.d. Silva).

https://doi.org/10.1016/j.ijpharm.2019.118466
Received 25 February 2019; Received in revised form 23 June 2019; Accepted 24 June 2019
Available online 26 June 2019
0378-5173/

promote the restoration of a stable ocular surface (Liang et al., 2009, Semeraro et al., 2014, Sharma et al., 2016).

Pirfenidone (5-methyl-1-phenyl-2-[1H]-pyridone) is therapeutic agent that exhibited anti-inflammatory, antifibrotic effects and modulation of cellular oxidation in animal experiments and clinical trials in idiopathic pulmonary fibrosis, renal fibrosis, and multiple sclerosis (Oku et al., 2002, Lederer et al., 2015, Yamagami et al., 2015, Khanum et al., 2017). Pirfenidone regulates a series of cytokines including TNFα and TNFβ's pathways (Misra and Rabideau, 2000). Its antifibrotic action is primarily attributed to its antagonism of fibroblast proliferation and migration and the reduction of extracellular matrix deposits (Lee et al., 1998, Lin et al., 2009). In the eye, pirfenidone has shown the prevention of corneal scarring, and the inhibition of orbital fibroblasts' migration (Lin et al., 2009). However, when was investigated the pharmacokinetics of 0.5% pirfenidone as a topically administered solution in eyes of rabbits, it exhibited a short half-life in cornea tissue (less than 19 min) as expected for ophthalmic formulations (Sun et al., 2011).

Drug bioavailability is one of the most difficult ways that researchers face because of the unique anatomy, physiology, and biochemistry of the eye (Gaudana et al., 2010). Most drugs administered on the ocular surface from solutions are rapidly drained by different mechanisms, such as blinking, tearing and tear dilution. In addition, different layers of the cornea, conjunctiva and sclera constitute a compact barrier for ocular penetration of drugs (Nagarwal et al., 2009). It is reported that 5%, or even less, of the dose administered, reaches intraocular devices (Hughes et al., 2005). To improve ocular bioavailability, various ophthalmic drug delivery systems, emulsions (Vandamme, 2002), nanoparticles (Vandamme, 2002) and liposomes (Agarwal et al., 2016) have been proposed. These systems can potentiate the bioavailability of the drugs facilitating transcorneal/transconjunctival penetration (Tamilvanan and Benita, 2004, Liu et al., 2016).

Monolein (MO) is a non-toxic, biodegradable and biocompatible amphiphilic lipid which, upon contact with water, forms spontaneously well-ordered liquid crystalline phases. In recent years, liquid crystal systems have received considerable attention because of their excellent potential as drug vehicles (Verma and Ahuja, 2016). The liquid crystal of MO has interesting properties for a topical delivery system, since, they have the ability to incorporate compounds independently of their solubility, their physical and enzymatic degradation, their controlled release, their ability to form gel *in situ* (Borgheti-Cardoso et al., 2015), and also they are bioadhesive (Lee and Kellaway, 2000, Shah et al., 2001, Esposito et al., 2005). The potential use for bioadhesive systems as drug carriers lies in its prolongation of the residence time at the absorption site, allowing intensified contact with the epithelial barrier (Hagerstrom et al., 2003). Those characteristics make these drug delivery systems interesting as new therapeutic tools in ocular administration.

Therefore, liquid crystalline nanoparticles may be a good candidate for pirfenidone ocular delivery because it could enhance the drug delivery topically. The objective of this study was to encapsulate pirfenidone in liquid crystal nanoparticles in order to increase the residence time of the drug in the corneal tissue, avoiding multiple daily doses.

2. Material and methods

2.1. Materials

Monoolein (MO), pirfenidone, poloxamer 407 (F127) and oleic acid were purchased from Sigma-Aldrich (St. Louis, MO). Ultrapure water was produced by a Milli-Q System (Millipore, Massachusets, USA). All other chemicals and reagents used in the study were of analytical or pharmaceutical grade.

2.2. Preparation of nanoparticles

The liquid crystalline nanoparticles pirfenidone was prepared through the top-down method (Guo et al., 2010). MO, oleic acid and Poloxamer 407 were firstly heated to 60 °C, and then pirfenidone solution at an appropriate concentration (0.5% w/w) was added to the molten MO (4.4% w/w)/Oleic acid (0.1% w/w)/Poloxamer 407 (0.5% w/w) and solubilized before adding to the aqueous phase (95% w/w). The mixture was heated to 60 °C, vortexed during 1 min, centrifuged at 1500*g* and repeated this cycle three times. Afterward, the sample was kept at room temperature until its homogenous state was achieved.

After equilibration of 24 h, a further reduction in size was achieved by treating the mixture for 10 min by probe sonication (500 Watt Ultrasonic Processors – VCX Series, Newtown, CT, USA) at 9 W energy input at 25 °C. Glycerol (0.9% v/v) was used to obtain the osmotic pressure to physiological conditions (295.7–308.3 mOsm/L) and the pH was adjusted to 7.0 with 0.1 M NaOH. Finally, the free drug was removed by centrifugal filter devices. Then the final concentration of pirfenidone was adjusted to 1 mg/mL. The formulation was stored at two different temperatures (4 °C and 25 °C), and protected from light. Blank nanoparticles (Blank-LCNPs) were prepared by the same process without adding the drug at the initial step.

2.3. Characterization of PFD-LCNPs

2.3.1. Particle size distribution, polydispersity index, and zeta potential

The particle size and polydispersity index of PFD-LCNPs were determined by dynamic light scattering (Zetasizer® Nanoseries ZEN3600, Malvern Instruments, Worcestershire, England) after adequate dilution (1:100, v/v) of an aliquot (1.5 mL) of the PFD-LCNPs in filtered water (0.45 mm, Millipore, Bedford, MA). For the analysis, a 1 cm wide polystyrene cell was used at a fixed angle of 90°.

The zeta potential (Zetasizer® Nanoseries ZEN3600, Malvern Instruments, Worcestershire, England) measurements were performed at 25 °C according to the electrophoretic mobility principle after diluting (1:100, v/v) of an aliquot (1.5 mL) of the PFD-LCNPs. All data sets were expressed in terms of the mean (±) standard error of the mean (SEM) of at least three different formulations. The determination of the hydrodynamic diameter, polydispersity index, and the zeta potential of the developed liquid crystalline nanoparticle formulations were performed 0, 15, and 30 days after the preparation.

2.3.2. Stability studies

The tendency toward the physical instability of the formulations was studied by multiple light scattering by means of evaluating the coalescence, creaming or flocculation (Turbiscan Lab®, Formulation, L'Union, France). Measurements were carried out during 28 days (day 0, day 15 and day 28) at 4 °C and 29 days (day 0, day 13 and day 29) at 25 °C to study the influence of temperature on the stability of the PFD-LCNPs and to determine the predominant mechanism of destabilization. The analysis was performed with undiluted samples for 1 h (one scan every 5 min) at 4 °C and 25 °C. The backscattering (BS) variation was the parameter evaluated since the transmission profile was close to 0% for all samples. The BS profile at t = 0 was used as the reference line and was subtracted from the profiles obtained in the subsequent measurements. The data were analyzed using Turbisoft® software to evaluate instability phenomena such as migration and particle size variation in these systems.

2.3.3. Morphology

The surface morphology of the PFD-LCNPs was determined by atomic force microscopy (AFM) and transmission electron microscopy (TEM). The samples were diluted in ultrapure water (1:100, v/v) and placed on a mica sheet, allowed to dry and imaged using a Cypher ES AFM (Asylum Research, USA) in amplitude and tapping mode. For the TEM analyzes, the samples were prepared by loading a 5 µL droplet of

the formulations onto a 300-mesh carbon-coated copper grid, and then the excess fluid was removed by an absorbent paper. These grids were kept in desiccators for 24 h before analysis by TEM and samples were observed using an FEI Tecnai G2-20 FEI SuperTwin 200 kV. Experiments and analyses involving electron microscopy were performed in the Center of Microscopy at the Universidade Federal de Minas Gerais, Belo Horizonte, MG, Brazil.

2.3.4. pH measurements

The pH values were determined in the undiluted PFD-LCNPs using a calibrated potentiometer (mPA-210 – Tecnopon, São Paulo, Brazil).

2.3.5. Polarized light microscopy (PLM)

Investigation of the phase behavior of both Blank-LCNPs and PFD-LCNPs was performed using a polarizing microscope. Micron-sized liquid crystalline particles were fabricated as described earlier but without the size reduction homogenization step. After that, a drop of the dispersion was placed onto a slide and imaged under a polarizing light microscope (Zeiss®, Model Axio Imager M2) at magnification power of 100x to evaluate the occurrence of birefringence.

2.3.6. Small-angle X-ray scattering (SAXS) measurement

Structural information was obtained through SAXS analysis. The experiments were performed at the SAXS-1 beamline at the Brazilian Synchrotron (LNLS, Campinas, Brazil). Liquid crystalline nanoparticles (Blank-LCNPs and PFD-LCNPs) were deposited on metal rings, which were sealed by a polyimide film (Kapton®) and impinged with an X-ray beam energy of 8.3 keV ($\lambda = 0.1488$ nm). A Pilatus 300 k detector was positioned 1.0 m from the sample, providing a reciprocal space vector range (Q) spamming from 0.15 nm^{-1} to 2.6 nm^{-1}. For all SAXS data, the 2D images obtained were normalized by the incoming beam intensity and sample's absorption and the background scattering contributions from sample chamber (mica) were subtracted and converted to intensity profiles I (Q) as a function of the scattering vector Q using the Fit2D software.

2.3.7. Encapsulation efficiency and drug loading

Encapsulation efficiency (EE %) and drug loading (DL%) were determined by high-performance liquid chromatography with ultraviolet detection (HPLC–UV). The HPLC system (Model 1260 Infinity Series, Agilent®, USA) consisted of a pump (model G1311B), the automatic injector (model G1329B), DAD detector (model G4212B) and Agilent® software (Model EZChrom Elite, USA). A C18 reverse phase column, 150 mm long and 4.6 mm in diameter and with 5 µm particles (Model LiChrospher® 100 RP-18 endcapped, Merck, Germany) was used. Sample (20 µL) was injected into the column with the mobile phase consisted of acetonitrile-water (35:65, v/v) with an isocratic flow rate of 1 mL/min and the UV absorbance detector operated at 311 nm with a retention time of 1.5 min.

The EE% and DL% were determined by ultra-filtration method using Microcon centrifugal filter devices (Millipore, Billerica, MA, USA). 0.5 mL PFD-LCNPs solution was transferred to the upper chamber of the centrifuge tube with a molecular weight cut-off of 100 kDa followed by centrifugation at 5000 rpm for 20 min. The ultrafiltration centrifugation method allows the separation of the non-encapsulated drug, which in turn was able to pass through the filter during centrifugation The pirfenidone concentration of the filtrate and original sample preparation (before filtration) were determined by HPLC at a wavelength of 311 nm. The linearity range of the calibration curve was within 1–500 µg/mL with a correlation coefficient of 0.9998. The drug encapsulation efficiency and drug loading were calculated according to:

$$EE\% = \frac{Wtotal - Wfree}{Wtotal} \times 100\%$$

$$DL\% = \frac{Wtotal - Wfree}{Wtotal - Wfree + Wemulsifier + Wlipid} \times 100\%$$

where, W_{total} is the total amount of drug in the nanoparticle; W_{free} is the amount of drug in the filtrate, W_{lipid} the amount of lipid and $W_{emulsifier}$ the amount of the emulsifiers. The data reported were expressed as the mean (±) standard error of the mean (SEM) of at least three different formulation measurements.

2.3.8. In vitro release profiles

The in vitro release of PFD-LCNPs was evaluated using the dynamic dialysis method. 1 mL of fresh PFD-LCNPs (1000 µg/mL) was loaded in a dialysis bag (MWCO 14,000 Da, Sigma, USA). The dialysis bag was then immersed in 52 mL release medium of simulated tear fluid (STF, NaCl 0.67%, $NaHCO_3$ 0.2%, $CaCl_2{\cdot}2H_2O$ 0.008%) at 37 ± 1 °C with stirring at 100 rpm. At predetermined time intervals, a 1 mL aliquot was withdrawn and immediately replaced with an equal volume of STF. PFD content in the release medium was quantified with an HPLC method similar to that of encapsulation efficiency determination. The cumulative amount of drug (Q_n, mg/mL) was plotted as a function of time (t, min) and calculated based on the following equation:

$$Qn = CnxVo + \sum_{i=1}^{n-1} CixVi$$

where C_n stands for the drug concentration of the dissolution medium at each sampling time, C_i is the drug concentration of its sample, and V_0 and V_i stand for the volumes of the dissolution medium and the sample, respectively.

2.4. In vitro study of ocular irritation

Ocular tolerability of PFD-LCNPs was evaluated by the Hen's Egg Test-Chorioallantoic Membrane test (HET-CAM test) described by Silva et al. (2019). This study is used as an alternative to the Draize rabbit eye test to check the ocular tolerance of the developed formulation using fertilized hen egg. Ten fertilized hen's eggs for each formulation were selected and handled to discard the defective ones. The eggs were incubated on an automatic rotating device (Premium Ecologica, Brazil) at 37 ± 1 °C and 60 ± 1% relative humidity, for 10 days. On the tenth day, the eggshell was opened at the side of the air chamber and the inner egg membrane was carefully removed to avoid any damage to the fine blood vessels of the chorioallantoic membrane (CAM). Ten days after fertilization, PFD-LCNPs (1 mg/mL, 100 µL), and PFD ophthalmic solution (1 mg/mL, 100 µL) was applied over the CAM surface. To evaluate the toxicity of the formulation components the same volume of a blank formulation was applied on the CAM (100 µL of Blank-LCNPs). As a negative control, the same procedure was performed and 100 µL of the vehicle (0.5% w/v carboxymethyl cellulose, CMC in 0.9% NaCl w/v) was applied over the CAM surface. At least, as a positive control, 100 µL of 0.1 M NaOH was applied over the CAM surface. After a 5 min' contact, the membrane was rinsed at 37 °C with phosphate buffered saline solution (PBS). Then, the blood vessels and the capillary system were examined for the post-application irritant effects of hyperemia, hemorrhage, and coagulation at different times (0, 0.5, 2 and 5 min). A time-dependent numerical score was then allocated to each formulation, and the sum of the time-dependent numerical scores for all three responses of hyperemia, hemorrhage, and coagulation was calculated and the mean sum of individual scores of all the endpoints from ten replicate assays gave a single numerical value, thus indicating the irritation potential of the formulation. The intensity of the reactions was semi-quantitatively assessed on a scale from 0 (no reaction) to 3 (strong reaction). The ocular irritation index (OII) was then calculated by the following expression:

$$OII = \frac{(301 - h)x5}{300} + \frac{(301 - l)x7}{300} + \frac{(301 - c)x9}{300}$$

where *h* is the time (in seconds) of the beginning of hemorrhage, *l* of lysis and *c* of coagulation, over a period of 300 s (5 min). The following classification was used: OII ≤ 0.9: slightly irritating; 0.9 < OII ≤ 4.9: moderately irritating; 4.9 < OII ≤ 8.9: irritating; 8.9 < OII ≤ 21: severely irritating.

2.5. Evaluation of corneal re-epithelialization

2.5.1. Animals

Female rabbits New Zealand, three weeks of age and weighing 2–3 kg were purchased from the Experimental Farm Professor Hélio Barbosa (Igarapé, Brazil). The animals remained in cages individuals throughout the period of adaptation (1 week) before experimentation, in an environment with an average temperature of 25 °C, constant and brightness varying according to sunlight. There was no restriction of water and food during the experiment and the used for evaluation. The study was approved by the commission on ethics on the use of animals of the Federal University of Minas Gerais (CEUA, Belo Horizonte, Brazil, Protocol n° 360/2018).

2.5.2. Corneal chemical burn by ethanol-exposed rabbit eyes

The method previously described by Mencucci et al. (2014) with some modifications was used. All procedures were performed with animals under general anesthesia, induced by an intramuscular injection of 50 mg/kg of ketamine hydrochloride (Dopalen®, Brazil) and 15 mg/kg of Xylazine hydrochloride (Anasedan®, Brazil).

The animals were divided into three groups of five rabbits each. The treatments were Blank-LCNPs (100 μL), PFD solution at 1 mg/mL (100 μL) and PFD-LCNPs at 1 mg/mL (100 μL), twice a day. Blank-LCNPs, PFD solution, and PFD-LCNPs were prepared freshly for every experiment to avoid the use of any preservative.

After ocular surface anesthesia by topical instillation of proxymetacaine (Anestalcon®, Brazil), a 9.0 mm Trephine blade (Katena, Denville, NJ) was placed and fixed firmly on the corneal surface with gentle pressure, then 100 μL of absolute ethanol was put into the well and left in place for 30 s and absorbed with a cotton pellet. Next, the eye was irrigated thoroughly with sterile PBS to remove all chemical residues. To finish, the epithelium was peeled using a blade along the boundary. All procedures of epithelial removal were performed on the right eyes of experimental animals. The treatments started immediately after surgery and for the following three days every 12 h. Precisely 100 μL of the formulation was placed into the conjunctival sac of the right eye and the eyes were manually closed for 10 s to allow the solution to be distributed over the cornea.

Fluorescein drops (Fluorescein Sodium 1.0%; Allergan®, USA.) were instilled into the study eye, and photographs were obtained using slit lamp (Apramed HS5, Brazil) under illumination with cobalt-blue light using a digital camera Canon EOS Rebel T5, (Canon, Inc., Tokyo, Japan). The area of corneal abrasion was measured semi-automatically with a custom macro written for ImageJ (Version 1.49; National Institutes of Health; USA). Measurements were corrected separately for each image using a calibration factor based on the photographs of the ruler.

2.5.3. Pre-ocular retention study

The pre-ocular retention of the PFD-LCNPs was assessed using a fluorescence imaging system (Zeiss®, Model Axio Imager Z2-ApoTome 2, Germany). This method makes use a property of pirfenidone which exhibits fluorescence in a range of excitation at 323–330 nm with an intense, sharp emission peak at 390–400 nm (Bruss et al., 2004). In order to evaluate the pre-ocular retention on the cornea, three female New Zeeland rabbits were used and received 100 μL of each formulation (Blank-LCNPs, PFD solution at 1 mg/mL and PFD-LCNPs at 1 mg/mL) using the same protocol as described before. After 1 h, the animals were euthanized using an overdose of barbiturate (sodium pentobarbital at a concentration of 81 mg/kg) and the corneal samples were removed and fixed immediately with 4% paraformaldehyde solution for 24 h. The samples were washed with PBS and incubated in sucrose solution before being included in OCT compound and frozen at −80 °C until the time of sections. Using cryostat (LeicaCM3050S), sections of 10 μm were made in the samples and then images were acquired from a fluorescence microscope with a 20× objective.

2.5.4. Histopathology

After 82 h of injury, the animals were euthanized and its eyes were removed. Corneal samples were obtained and fixed in Dawidson's solution (two parts of 10% neutral phosphate-buffered formalin, three parts of 95% ethanol, one part of glacial acetic acid and three parts of ultrapure water) for 24 h, then the corneal tissue was placed in 70% ethanol per 12 h, embedded in paraffin, cut at 4 μm and stained with hematoxylin and eosin. The histological analysis was performed using an optical microscope (Zeiss®, Model Axio Imager M2).

2.5.5. Myeloperoxidase (MPO) and N-acetylglucosaminidase (NAG) measurements

Initially, using ice-cold Buffer 1 solution (0.1 M NaCl, 0.02 M Na_3PO_4 and 0.015 M Na_2EDTA) 20 mg of cornea were homogenized and centrifuged at 4 °C for 10 min at 10,000 RPM. The supernatant was discarded and the pellet was resuspended in 0.2% NaCl solution and 1.6% NaCl plus 5% glucose. Then, the procedure was repeated one more time. The supernatant was discarded and the pellet resuspended in Buffer 2 (Na_3PO_4 and 0.5% Hexadecyltrimethylammonium bromide w/v, HETAB) solution. For the quantification of Myeloperoxidase (MPO), the samples were frozen in liquid nitrogen and unfreeze in the water at room temperature. This procedure was performed three consecutive times. The samples were centrifuged for 15 min at 10,000 RPM (5000*g*) at 4 °C. To perform the enzymatic assay an aliquot of the supernatant was removed for dilution in Buffer 2. The sample was plated in triplicate in one microplate. 3,3′, 5,5′-Tetramethylbenzidine (TMB substrate), previously diluted in Dimethyl sulfoxide (DMSO), was added. During 5 min the plate was placed in an oven at 37 °C. Then H_2O_2 (0.002%) was added and the samples were again incubated at 37 °C for 5 min. After the incubation, the reaction was stopped with the addition of H_2SO_4 (1 M, 100 μL). The absorbance reading was at 450 nm. The mean of the values obtained in each triplicate was used to determine the activity of the enzyme.

For indirect quantification of N-acetylglucosaminidase (NAG) activity (Assay Kit by Sigma Aldrich) in macrophages, 20 mg of corneal tissue was homogenized with saline/Triton solution (Saline 0.9% and Triton x-100, 1%) and then centrifuged at 4 °C for 10 min at 3000 RPM (1500*g*). The supernatant was collected and diluted in phosphate-citrate buffer (0.1 M citric acid and 0.1 M Na_2HPO_4) to proceed with the NAG assay. 100 μL of each diluted sample was plated in triplicate. Then was added the substrate p-nitrophenyl-N-acetyl-β-D-glucosaminidase (2.2 mM), diluted in a phosphate-citrate buffer. During 5 min the plate was placed in an oven at 37 °C. After the reaction, 0.2 M of glycine buffer was added to the samples to paralyze the reaction. The absorbance reading was performed at 405 nm. The mean of the values obtained in each triplicate was used to determine the activity of the enzyme.

2.6. Data analysis

Means ± SEM is shown for the number of independent experiments indicated in Figure Legends. GraphPad PrismTM software was used to analyze data for statistical significance performed using a one-way analysis of variance (ANOVA), followed by Bonferroni post-hoc multiple comparison testing and considered statistically significant ($p < 0.05$).

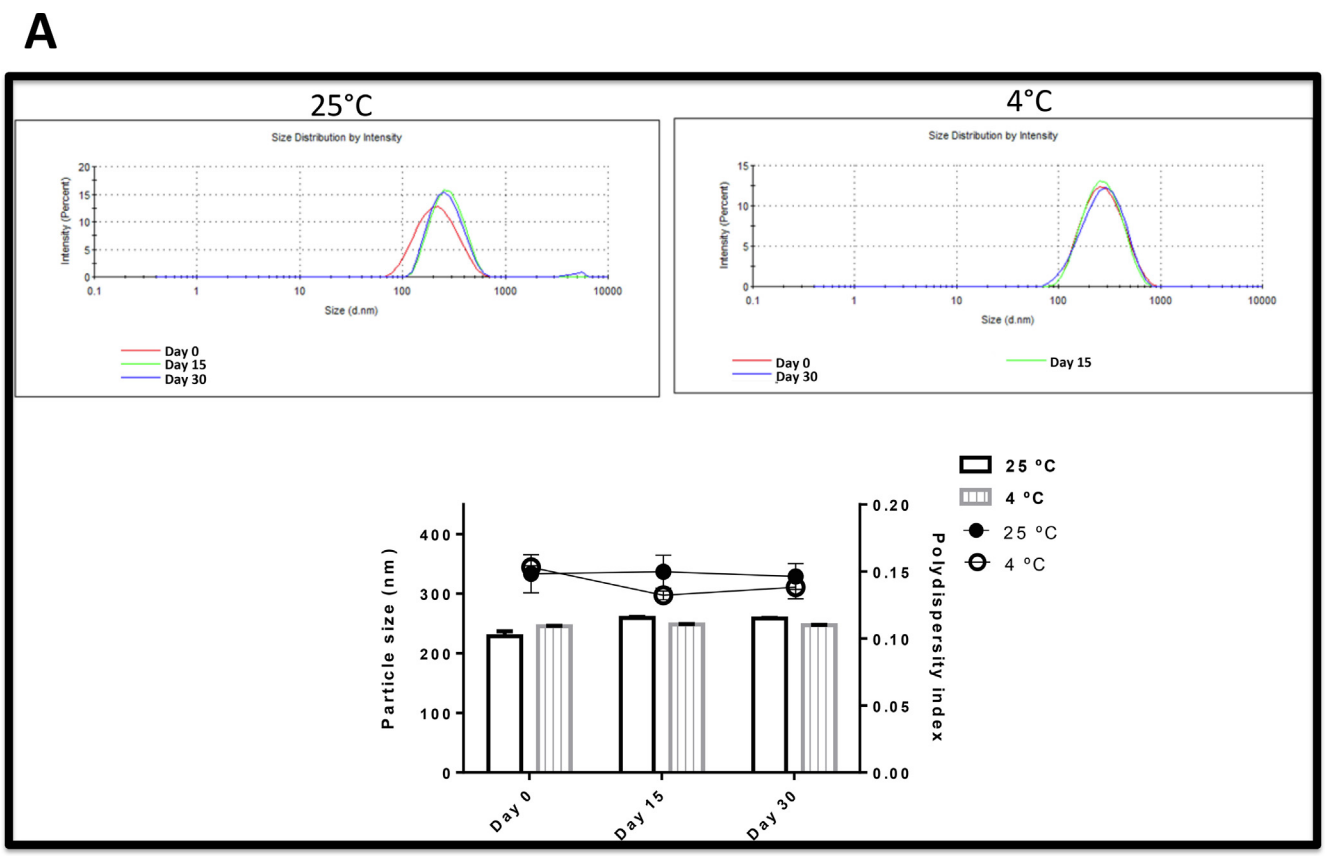

Fig. 1. (A) Particle size distribution of nanoparticles stored at 4 °C and 25 °C over 30 days. (B) Zeta potential distribution of nanoparticles stored at 4 °C and 25 °C over 30 days. (C) the pH of nanoparticles stored at 4 °C and 25 °C over 30 days. All determinations were performed in triplicates. Statistical analyses were performed: *indicates $p < 0.05$ when compared to day 0.

3. Results and discussion

3.1. Particle size distribution, polydispersity index, zeta potential and pH measurements

The size of the particles is a valuable factor in the evaluation of physicochemical stability, in-vivo absorption, and bioavailability of delivery systems (Rezvani et al., 2018). During the period evaluated for formulations stored at 4 °C the measured mean hydrodynamic diameter and polydispersity index (PDI) were 247,3 ± 0,599 nm and 0,1200 ± 0,006, respectively (Fig. 1A). There were no statistically significant changes in both parameters, diameter and polydispersity index of the formulations. When the formulations stored at 25 °C was evaluated the measured mean hydrodynamic diameter and PDI were 257,5 ± 5,568 nm and 0,1620 ± 0,009, respectively. There were statistically significant variations in particle size after 15 and 30 days, which could be attributed to the phenomena of particle aggregation over 30 days. The value of PDI in all measurements was lower than 0.2, which suggests unimodal and homogeneous distribution of the particles (Danaei et al., 2018). The PDI did not undergo major changes over the 30 days, this indicates that although the mean size is varying for the formulations stored at 25 °C, the homogeneity a remains stable.

The zeta potential values measured after preparation, 15 and 30 days of all formulations were presented in (Fig. 1B). When evaluated the formations stored at 4 °C the zeta potential was −33,60 ± 1,06 mV and none of the samples presented a statistically significant variation in the value of this parameter in the period evaluated. However, for the formulations stored at 25 °C, the zeta potential was −46,00 ± 2,45 mV and there was statistical variation after 15 and 30 days of the preparation with reduction of the zeta potential. All PFD-LCNPs that were formulated and stored at the two different temperatures showed a negatively charged zeta potential, which could be expected due to the presence of exposed carboxylic groups of oleic acid and adsorption of free hydroxyl groups on the surface of PFD-LCNPs (Abdelaziz et al., 2019).

Zeta potential is an important physicochemical parameter that influences the stability of formulations. As a rule of thumb, absolutes zeta potential values above 30 mV provide good stability and in the other hand values in the range −5 mV to +5 mV indicate fast aggregation (Patel and Agrawal, 2011). Large repulsive forces being positive or negative tend to avoid aggregation due to occasional collisions of adjacent nanoparticles (Bhattacharjee, 2016). Together, these parameters indicate that the temperature of 4° C retains the nanoparticles of liquid crystal, which were less aggregated as evidenced in the analyzed parameters.

The pH is a key factor in determining the permeability of the cornea to a drug (Pahuja et al., 2012). There is a delicate balance therefore between aiming for a pH appropriate for corneal penetration and the physiological pH (7.4), which will result in the least tearing. The pH comfort zone for topically administered ophthalmic medication is quite narrow, ranging from 6.5 to 7.8 (Awwad et al., 2017). The pH value of the liquid crystal nanoparticle formulation at temperatures of 4 °C and 25 °C was 6.910 ± 0.0194 and 6.920 ± 0.0079, respectively. Thus, the pH was considered adequate for the proposed use because it is close to the pH of the lacrimal liquid allowing the necessary comfort of a formulation for topical ocular use. Also, at this pH, the pirfenidone molecule is neutral (not ionized) with high solubility in aqueous medium and is able to travel through cell membranes without requiring a receptor, which favors a greater bioavailability facilitating its permeation through the tissue (Shi et al., 2007). There were no statistically significant changes in pH values over the period-evaluated (Fig. 1C).

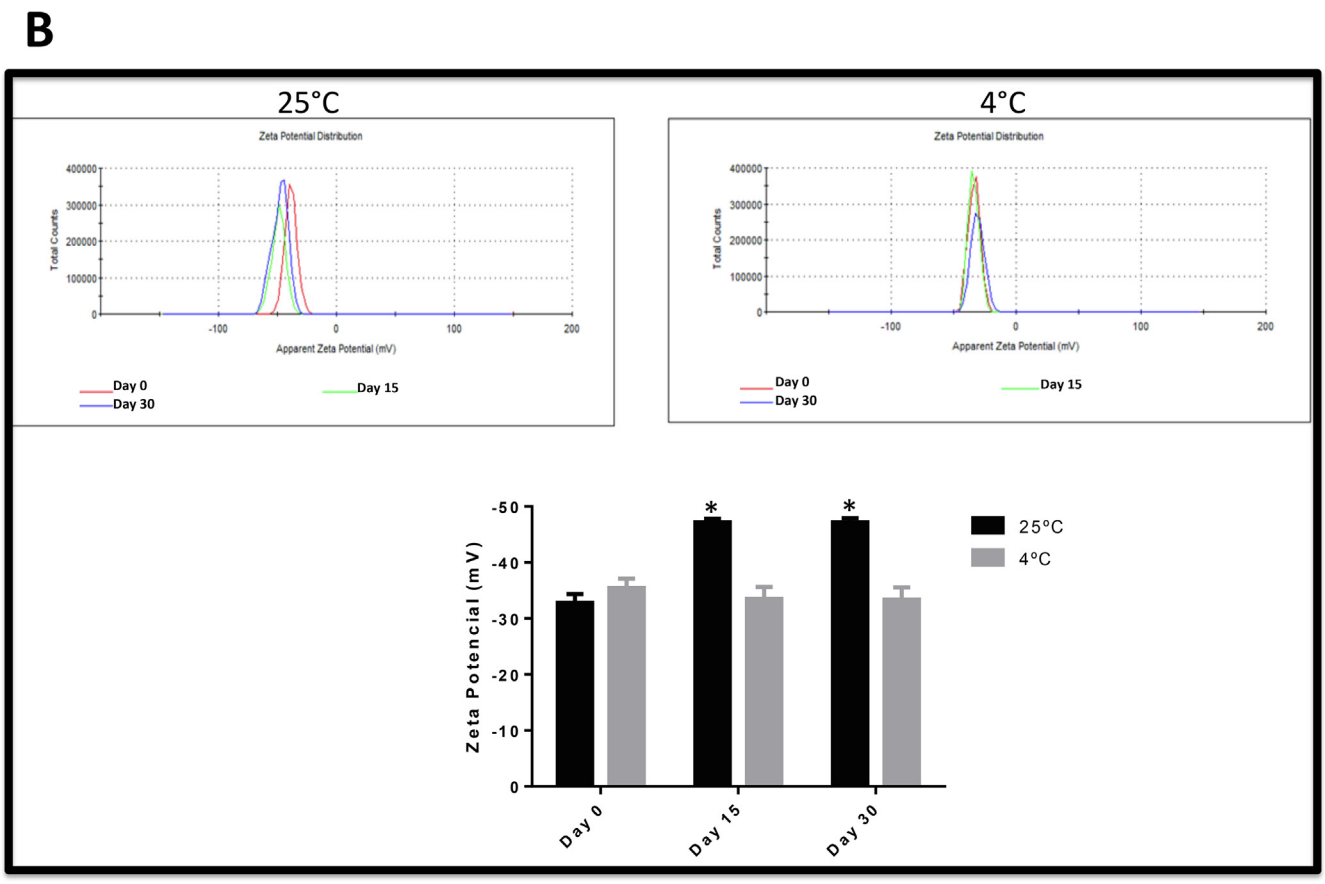

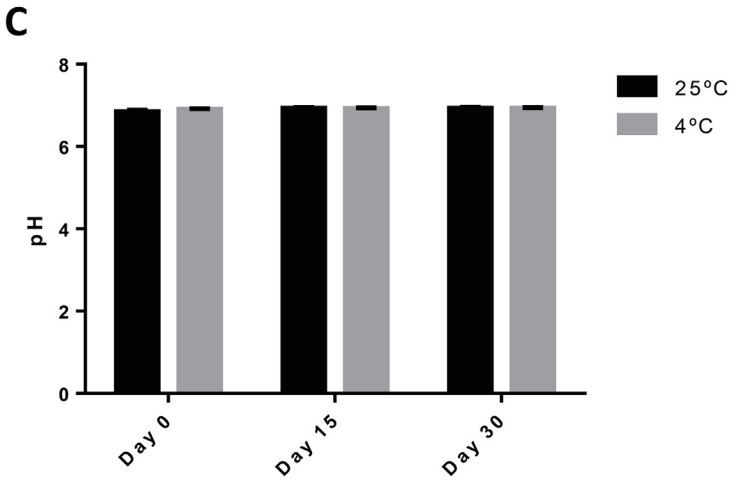

Fig. 1. (*continued*)

3.2. Stability studies

The graphs obtained from the optical characterization analyzes by multiple light scattering are shown in Fig. 2. This instrument is capable to detect destabilization by creaming before it is visible by the naked eye (Trujillo-Cayado et al., 2014). For the formulation stored at 4 °C the Backscattering (BS) profile indicates that there was a slight increase in particle concentration at the base (red line) over the course of the 28 days evaluated and a reduction of the particles at the top of the cuvette. In the middle of the cell, the spectra presented a high overlap, with a variation lower than 2%, demonstrating that the slope of BS for PFD-LCNPs over 28 days of incubation (Fig. 2A) was not significantly modified during analysis, which corroborates with the particles size analyzes performed during the same time interval (Fig. 1A). None of the detected variations was greater than 10%, suggesting that there were no irreversible destabilization processes and that stable formulations were obtained (Celia et al., 2015). This observation could be attributed to an appropriate size and zeta potential of the nanostructures providing strong electrostatic repulsion and physical stability over time.

However, when the formulation stored at 25 °C was evaluated, the Backscattering (BS) graph showed negative variations of more than 20% at the base of the cell and 15% at the top just after 13 days of storage (Fig. 2B). This indicates a reduction in the concentration of particles in the base and increases in the top of the cell (cremation) (Celia et al., 2009). Moreover, the final backscattering level (blue line) at a height of 3 mm changes from −4% at time 0:00 to −26% after

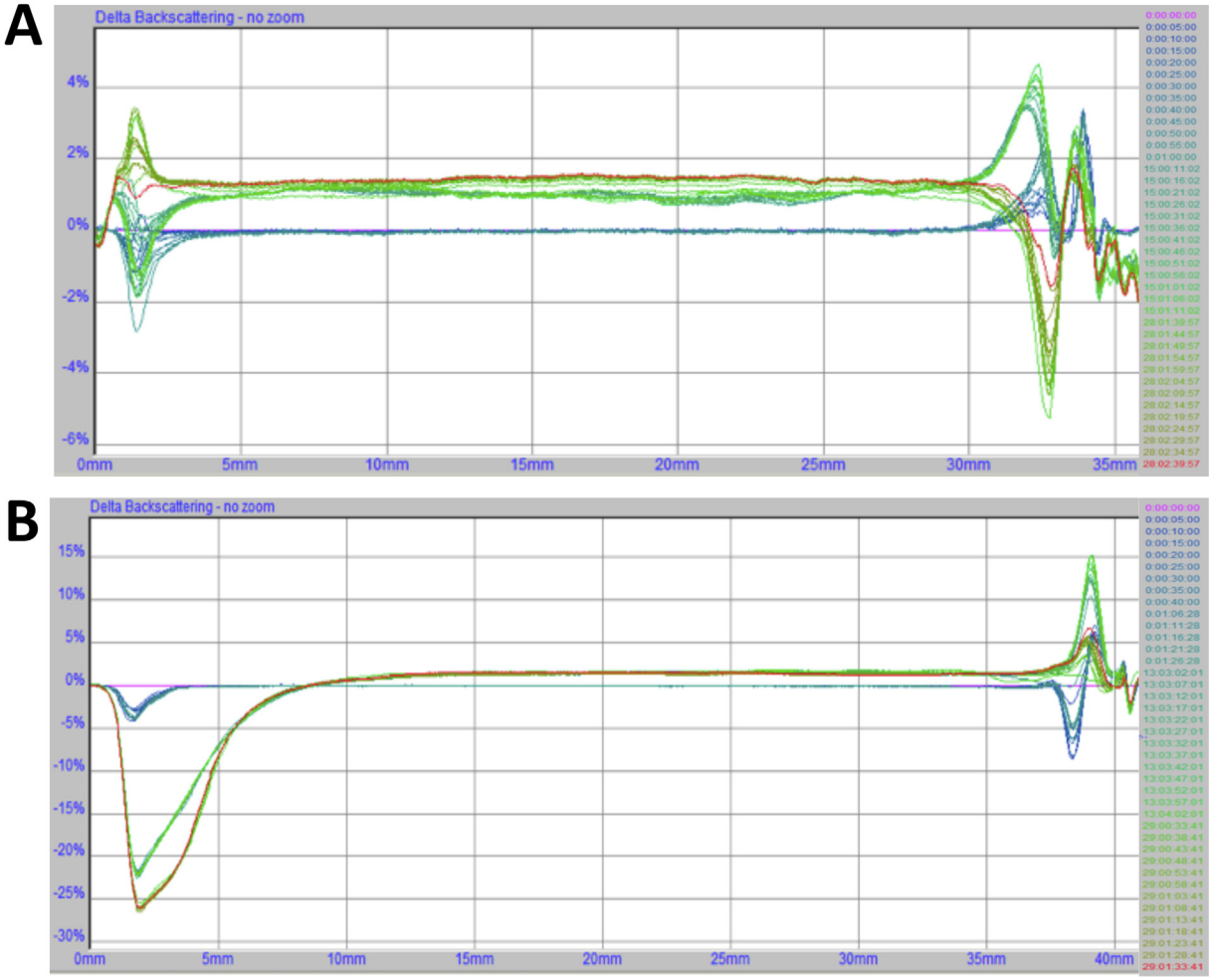

Fig. 2. Micrographs of PFD-LCNPs taken using atomic force micrograph (A) and transmission electron micrograph (B).

29 days (red line), while at 38 mm there is a change from −9% to 15% demonstrating a high creaming rate of the formulation stored at 25 °C (Wiśniewska et al., 2016). It corroborates with the variation of particle size performed during the same time interval (Fig. 1A) under the same storage conditions. The results of multiple light scattering (Turbiscan) and dynamic light scattering supported each other. Taking into account these results, the PFD-LCNPs stored in 4 °C presented the best physical stability on account of the evolution of its mean particle sizes.

3.3. Morphology

Both AFM and TEM (Fig. 3) pictures show spherical PFD-LCNPs having a smooth surface without any evident irregularities and separated from each other, suggesting possible stabilization of the NPs due to negative surface charges. These findings indicated the successful formation of PFD-LCNPs. Transmission electron microscopy (TEM) and atomic force microscope (AFM) are an indispensable tool for use in many fields of nanotechnology research and development, including the investigation of drug nanocarriers enabling the detection of alterations in nanoparticle morphology (Manaia et al., 2017). It becomes apparent that a major difference between some of the methods applied is the question of nanoparticle environment. In some methods, the samples can be measured while freely moving in solution (DLS), while for others, they must be dried, or even placed in a high vacuum before measurement (TEM and AFM) (Eaton et al., 2017).

3.4. Polarized light microscopy (PLM)

Anisotropic systems cause a deviation in the plane of polarized light (birefringence, similar to real crystals), resulting in typical black and white images, or colored textures (Manaia et al., 2017). Fig. 4 shows the micrographs of PFD-LCNPs and Blank-LCNPs under a polarized light microscope. The appearance of this pattern is similar to the fan-shaped texture, which is typical for hexagonal liquid crystalline structure (Rossetti et al., 2011, Rodrigues et al., 2016). The hexagonal structure presents faster adsorption kinetics and greater free energy gain after the adsorption of the particle on a surface. This means that the nanoparticles in this phase (hexagonal) spread more easily than the particles in the cubic phase for example, which leads to greater coverage in the applied area (Landau and Rosenbusch, 1996).

3.5. Small-angle X-ray scattering (SAXS) measurement

It is important to improve the understanding of how chemical and structural properties of structured nanoparticles affect interactions and functionalities in biological systems. Such information directly impacts the design of drug-delivery vehicles of active pharmaceutical substances (Vandoolaeghe et al., 2009).

Fig. 5 shows the small angle x-ray scattering profiles for the PFD-LCNPs sample and the Blank-LCNPs sample. One notices the absence of a form factor for low q-values, with a monotonic decrease of the measured intensity. A clear and broad intensity hump is observed near $q = 1.6\,nm^{-1}$, followed by a smooth decay towards background level counts. The observed hump on each curve is related to the nearest

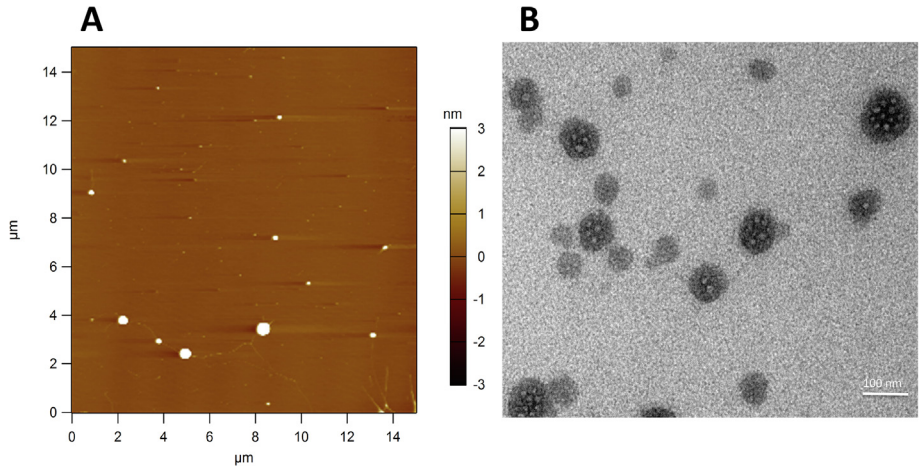

Fig. 3. Photomicrograph of a hexagonal liquid crystal using polarized light microscopy.

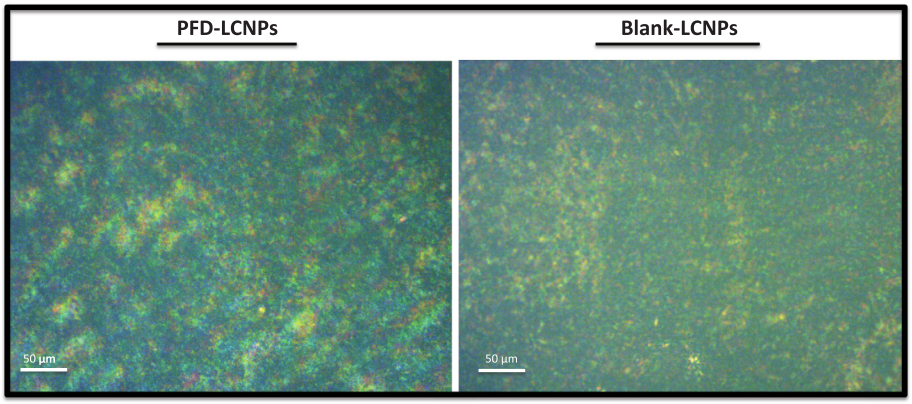

Fig. 4. SAXS profiles of the PFD-LCNPs loaded with pirfenidone at 1 mg/mL and Blank-LCNPs.

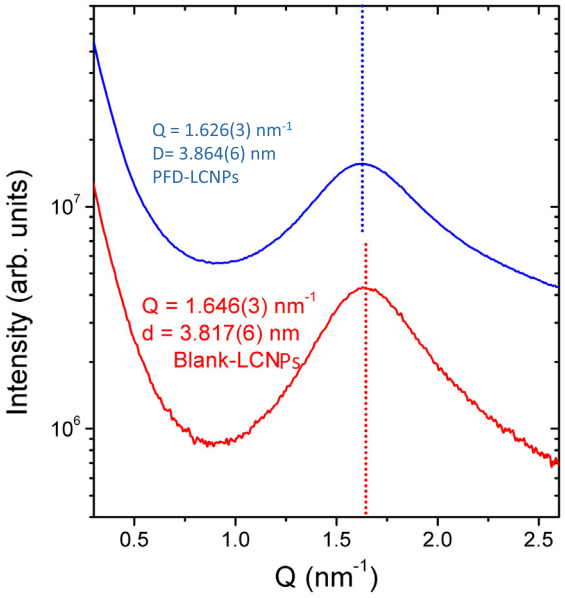

Fig. 5. In vitro release profiles of pirfenidone released from a PFD solution and from PFD-LCNPs (n = 3).

neighbor (first order peak) of the molecular packing of both systems, which assumes lower q-values for the PFD-LCNPs sample (peak at $q = 1.626\ nm^{-1}$), with respect to the Blank-LCNPs system (peak at $q = 1.646\ nm^{-1}$). The corresponding nearest-neighbor distances in real space of d = 3.817 nm and d = 3.864 nm for the Blank-LCNPs and PFD-LCNPs, respectively, indicate that the inclusion of pirfenidone leads to an expansion of 1.2% in the molecular packing in the PFD-LCNPs system. The presence of pirfenidone may be interfering in the ordering of monoolein both for the tails and for the headgroups (including hydroxyl and carbonyl groups). It is believed that, due to its molecular structure (with high permeability and high solubility), pirfenidone may generate an imbalance between the hydrophobic chains and headgroup (Mishraki et al., 2011). The Addition of the pirfenidone may a sizeable effect on the axial tilt angle distribution. This indicates the fact that the drug disrupts the tighter packaging of the lipid layer when compared to Blank-LCNPs, inducing the observed 1.2% expansion of the molecular packing.

3.6. Encapsulation efficiency and drug loading

The drug loading could reach 6.0 ± 1.82% along with 35.9 ± 2.09% encapsulation efficiency when adding 0.5% w/w of PFD. The lower encapsulation efficiency observed may be associated with a dilution of the drug due to the large proportion of water in the formulation. Another reason may be associated with the reduction of drug loading is a high-energy used for the particle size reduction (sonication) step leading to the drug exit from the system (Li et al., 2013). Also, the moderate entrapping efficiency of pirfenidone is related to its good solubility in water and its LogP (1.9), which makes it difficult for the drug to remain trapped in the nanoparticle that presents lipophilic characteristics (Macias-Barragan et al., 2010).

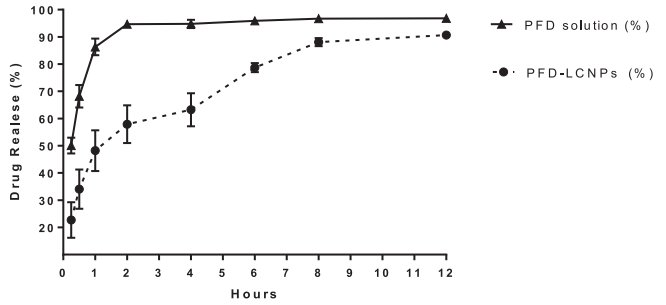

Fig. 6. Backscattering profiles at 25 °C of PFD-LCNPs analyzed by the Turbiscan Lab® equipment, within a period of up to 29 days after preparation. (A) PFD-LCNPs stored at 4 °C. (B) PFD-LCNPs stored at 25 °C.

3.7. In vitro release profiles

The in vitro release studies of drug delivery systems predict their *in-vivo* behavior and reach the goal of controlled release. In the present work, in vitro release studies were conducted in pH 7.4 to simulate the tear fluid. As Fig. 6 presents, PFD in solution was almost completely released within 2 h (94% drug release) while at the same time, PFD-LCNPs exhibited a 58% release indicating that such formulations showed greater control in the release of the active. It was found that 50% of PFD in water solution released after 15 min and almost 90% after 1 h, which suggested that PFD could freely diffuse through the dialysis membrane. The solubility and permeability profiles suggest that pirfenidone is a Biopharmaceutics Classification System (BCS) Class 1 (log D of 1.37 ± 0.05) drug with high permeability and high solubility (Trivedi et al., 2012). Thereby, the PFD is a hydrophilic drug, adsorbed onto the surface of nanoparticles, would easily diffuse from the matrix. This characteristic of the pirfenidone could justify the initial burst of the PFD-LCNPs in which it released 23% of the drug in 15 min. In addition, PFD release occurred primarily through the water channel of unique hexagonal structure (Hyde et al., 1984), which was indicates by PLM (Fig. 4).

3.8. In vitro study of ocular irritation

The chorioallantoic membrane of the chick embryo has complete tissues including arteries, veins, and capillaries, giving a similar result as conjunctival tissue on inflammation (Warren et al., 1990). The Blank-LCNPs, PFD solution, PFD-LCNPs, 0.9% NaCl + CMC 0.5% (negative control) and 0.1 M NaOH (Positive control) were tested for their irritation potential and then irritation score was measured up to 5 min (Fig. 7). The results showed, on Table 1 below, that Blank-LCNPs, PFD solution, PFD-LCNPs and 0.9% NaCl + CMC 0.5% (negative control) were practically non-irritating (score ≤0.9), whereas 0.1 M NaOH solution showed coagulation implied that the solution produced irritating effects (score 19.53). From the study, it was concluded that components of PFD-LCNPs is non-irritant and well tolerated for ocular administration.

3.9. Evaluation of corneal re-epithelialization time

It has been shown that the rabbit cornea is similar in size to the human cornea, which confirms its suitability of the model for translational research (Imanishi et al., 2000). In addition, the rabbit cornea responds to a large degree comparable to the human cornea in respect to wound healing time, the extent of scarring, and myofibroblast formation (Stepp et al., 2014). The photographs of corneas under cobalt-blue light after fluorescein staining are shown in (Fig. 8A), and the healing progress is measured in (Fig. 8B). Rabbit eyes (n = 5 per group) were treated with vehicle alone (Blank-LCNPs), PFD solution at 1 mg/mL, 100 μL and PFD-LCNPs at 1 mg/mL, 100 μL. During the first 60 h, no difference in the healing pattern of the corneal lesions of the animals was observed. However, after 72 h the animals that receive the vehicle had a lesion reduction of 52% while the group treated with PFD-LCNPs at 1 mg/mL had an 84% reduction of the wound (*$p < 0.05$). Later, at 84 h after corneal chemical burn, animals treated with PFD-LCNPs at 1 mg/mL and Blank-LCNPs exhibited reductions in corneal lesions of 91% and 54%, respectively (***$p < 0.01$). This indicated significant improvement in the healing process in PFD-LCNPs treated eyes. Meanwhile, no significant differences in healing were observed between the vehicle and the group treated with PFD solution at 1 mg/mL as well as no statistically significant difference between PFD-LCNPs at 1 mg/mL and PFD solution at 1 mg/mL (Fig. 8B). It is possible to observe that after 72 h of PFD-LCNPs administration a possible equilibrium concentration was reached which led to the desired therapeutic effect (corneal re-epithelialization). This demonstrates that the PFD-LCNPs increased the time of contact between the drug and the cornea, which is not observed in the groups treated with the PFD solution due to high clearance of the drug as shown in Fig. 9.

Similar results of the good reepithelization process were found administering 20 μL an eye drop formulation containing 5 mg/mL of pirfenidone encapsulated in PLGA 50:50 one per day during 7 days, after damage to the cornea of a rabbit by alkali burn (Chowdhury et al., 2013). Corneal re-epithelialization time was significantly reduced in pirfenidone encapsulated in PLGA nanoparticles treated eyes compared to the control eyes (group treated with vehicle Blank-PLGA nanoparticles) after 7 days. Similarly, using a cornea alkali-burned model in rat, it was administrated topically 10 μL of pirfenidone (1 mg/mL) dissolved in phosphate buffered saline (PBS) four times per day for 14 days. Corneas wound of the pirfenidone group were close to healed on day 7, while cornea wound of the group treated with vehicle (PBS) was still obvious (Jiang et al., 2018). Pirfenidone counteracted the TGF-β induced cell cytostatic effect, which might have enhanced the proliferation of corneal epithelial cells, resulting in more rapid re-epithelialization. Furthermore, in an in vitro study using Tenon's fibroblasts was demonstrated that pirfenidone downregulated the expression of TGF-β1, -β2, and -β3 (Lin et al., 2009). Rapid re-epithelialization helps to re-establish the corneal homeostasis and prevent further damage to the underlying stroma. Therefore, a reduction in corneal re-epithelialization time is an indicator of enhanced healing. In light of these findings, we proved that the installation of PFD-LCNPs at 1 mg/mL twice daily improves corneal wound healing and therefore provide a potential therapy to mediate corneal chemical burns.

3.10. Pre-ocular retention study

The pharmacokinetic profile of pirfenidone after topical administration to rabbit eyes (250 mg/mL, 50 μL) was observed in corneal tissues exhibiting short terminal half-life of 18 min (Sun et al., 2011). Topical ocular drug administration usually allows only a short contact time on the ocular surface. As shown in (Fig. 9B), after 1 h, nearly no fluorescence was observed in the PFD solution, and only a small amount of fluorescence intensity remained in the epithelium of the cornea. However, when the eyes were instilled with PFD-LCNPs, strong fluorescence intensity was observed in the epithelium during the period of 1 h, as shown in (Fig. 9A), compared to the vehicle (Blank-LCNPs). It is also possible to observe that the diffusion of the drug was not as rapid in the pre-corneal region and permeation of the drug into the stroma layer, proving that the PFD-LCNPs increase the perfusion of the drug.

These results indicate that the application of the PFD-LCNPs resulted in relatively strong fluorescence intensity and slow clearance from the PFD. The fact that the PFD-LCNPs is a hexagonal phase helps in the best spreadability, which leads to better coverage of the surface of the injured cornea. In conclusion, the PFD-LCNPs promoted a long time of contact of the drug with the corneal epithelium, which increased the ocular residence time of the drug on the corneal surface.

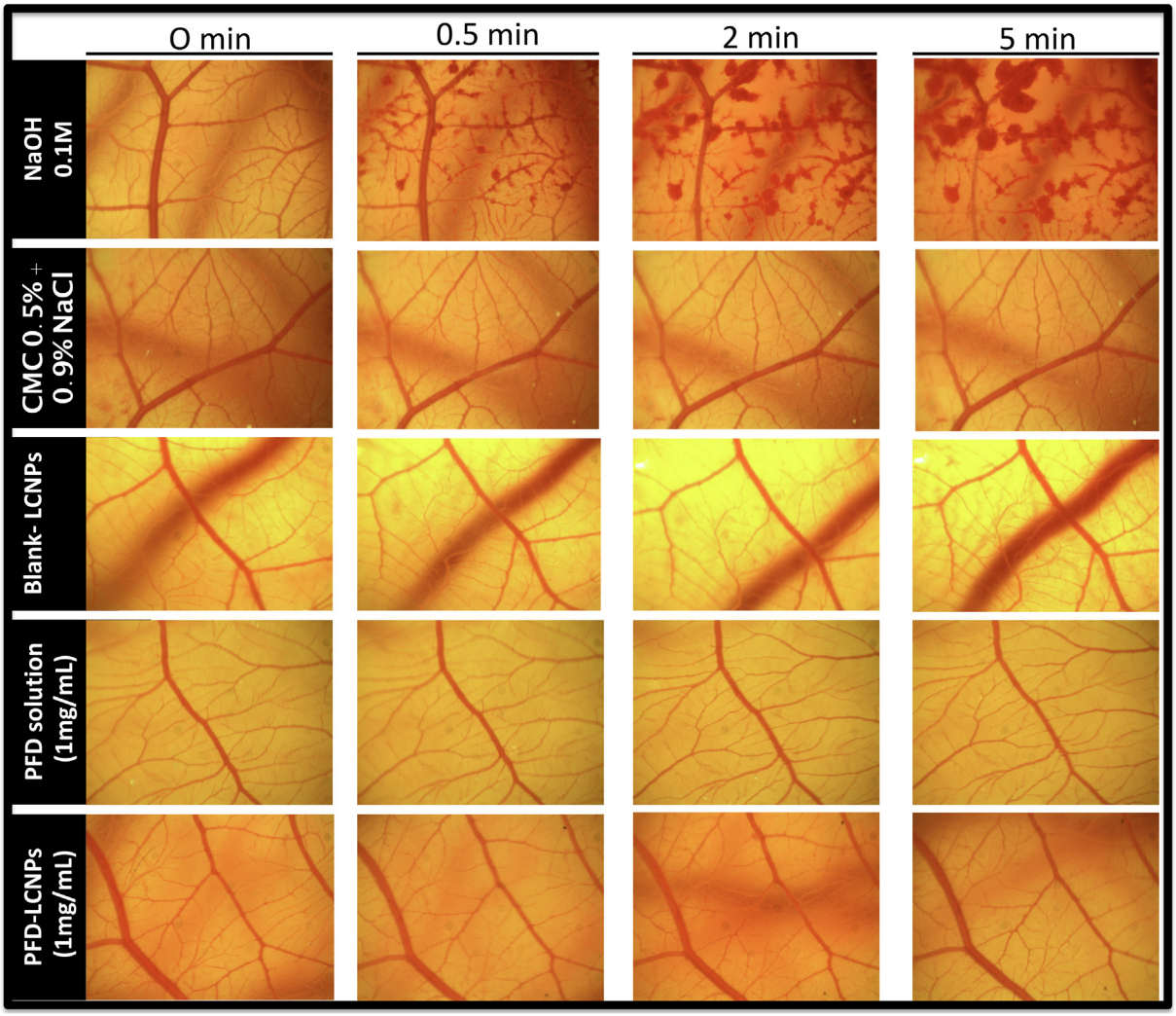

Fig. 7. Sequence of photographs illustrating the effect of 100 µL 0.1 M NaOH (Positive control), 0.9% NaCl + CMC 0.5% (negative control), Blank-LCNPs (vehicle), PFD solution at 1 mg/mL and PFD-LCNPs at 1 mg/mL on the membrane over a 5-min period.

Table 1
Ocular irritation index (OII) scores for the tested PFD-LCNPs.

Tested solution/dispersion	Score ± SEM	Irritancy classification
M NaOH, 100 µL (Positive control)	19.53 ± 0.05	SI**
0.9% NaCl + CMC 0.5%, 100 µL (Negative control)	≤0.9 ± 0.0	NI*
Blank-LCNPs (vehicle), 100 µL	≤0.9 ± 0.0	NI*
PFD solution – 1 mg/mL, 100 µL	≤0.9 ± 0.0	NI*
PFD-LCNPs – 1 mg/mL, 100 µL	≤0.9 ± 0.0	NI*

* NI-Non-irritant or slightly irritant.
** SI-Severely irritant. The results are expressed as mean ± SEM. (n = 10).

3.11. Histopathology

Histological evaluation of corneal epithelium done after the 84 h injury is shown in Fig. 10. Animals treated with PFD solution at 1 mg/mL, 100 µL and PFD-LCNPs at 1 mg/mL, 100 µL evidenced stroma with normal fibrocytes and its surface was epithelialized with six to seven layers, and more organized collagen bundles aligned parallel in the stromal layer when compared with animals treated with vehicle alone. In addition, the group vehicle-treated animals showed small granulation and inflammatory infiltrates when compared with animals treated with pirfenidone. PFD was originally shown to be an anti-fibrotic agent, and after being examined in detail for idiopathic pulmonary fibrosis, it exhibited substantial anti-inflammatory properties (Bayhan et al., 2016).

3.12. Myeloperoxidase (MPO) and N-acetylglucosaminidase (NAG) measurements

Myeloperoxidase (MPO) is a heme-containing peroxidase synthesized during myeloid differentiation that constitutes a major component of neutrophil azurophilic granules, has been extensively used as a marker for measuring polymorphonuclear leukocytes accumulation in tissue samples (McCormick et al., 2012). N-acetylglucosaminidase (NAG), present in lysosomes, has been employed to detect macrophage accumulation/activation in a variety of animal and human tissues demonstrated increases in polymorphonuclear and macrophage infiltration after inducing corneal alkali burn in mouse (Belo et al., 2004; Okada et al., 2016).

As illustrated in Fig. 11A, MPO activities were lower in animals treated with PFD-LCNPs at 1 mg/mL compared to the Blank-LCNPs ($p < 0,034$). Furthermore, there were statistically significant with animals treated Blank-LCNPs and healthy animals ($p < 0,026$). We found lower MPO activity in animals that had a corneal chemical injury that was treated with PFD-LCNPs at 1 mg/mL, which reflects the reduction of neutrophil accumulation in this region after 84 h. PFD exerts its effects by reducing the levels of inflammatory cytokines, such as

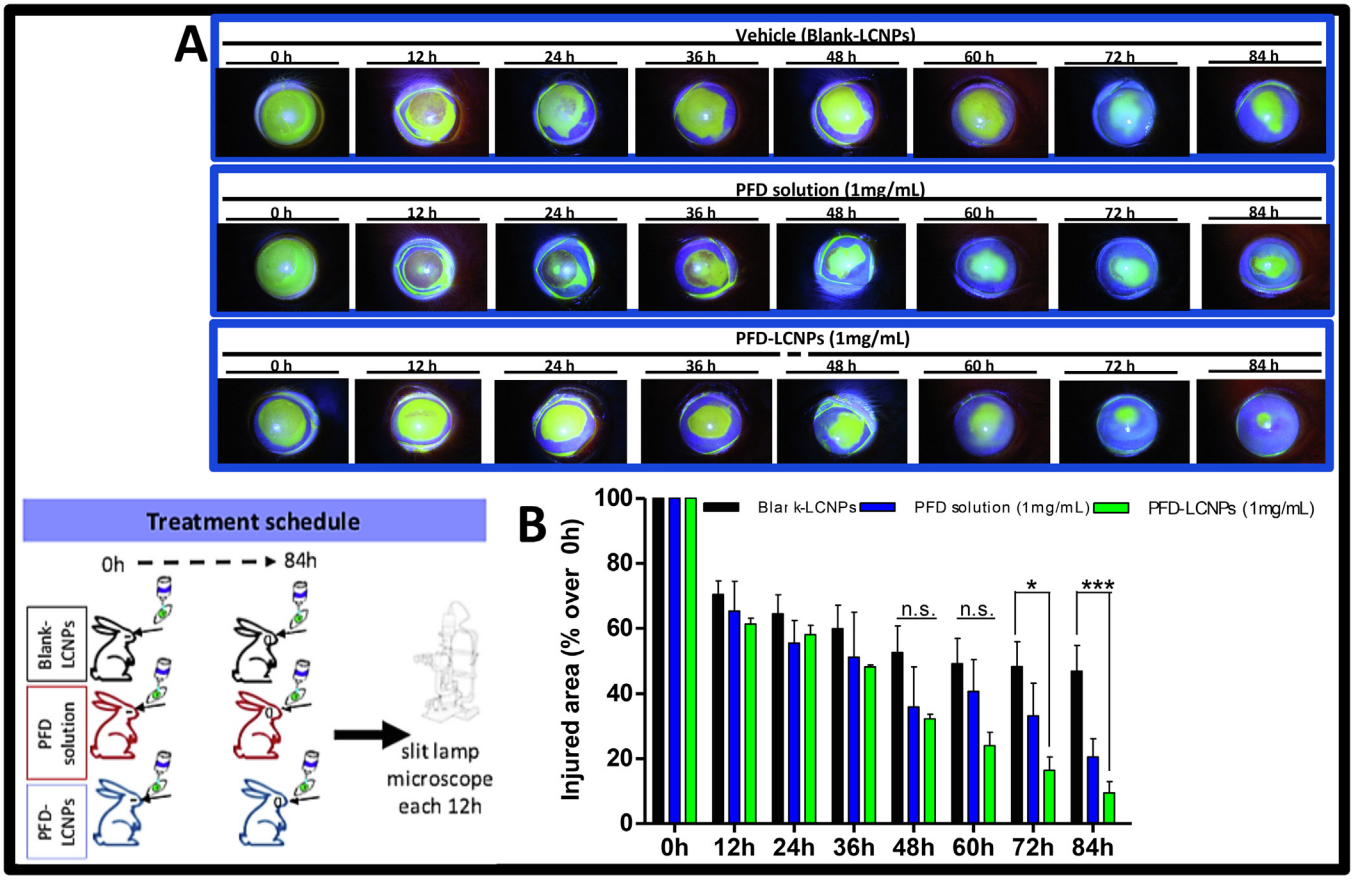

Fig. 8. Effect of PFD-LCNPs at 1 mg/mL on corneal healing after chemical burn: (A) Representative pictures of Blank-LCNPs (vehicle), PFD solution and PFD-LCNPs treated corneas after 12, 24, 48, 60, 72 and 84 h of injury. (B) Graph shows the corneal reepithelialization time: Corneal re-epithelialization time was significantly (*$p < 0.05$) reduced in PFD-LCNPs at 1 mg/mL treated eyes compared to the group treated with vehicle (Blank-LCNPs) after 60 h, but the corneal re-epithelialization time in PFD solution at 1 mg/mL treated eyes was not significantly different from the group treated with vehicle alone (Blank-LCNPs). Data are expressed as mean ± SEM, n = 5.

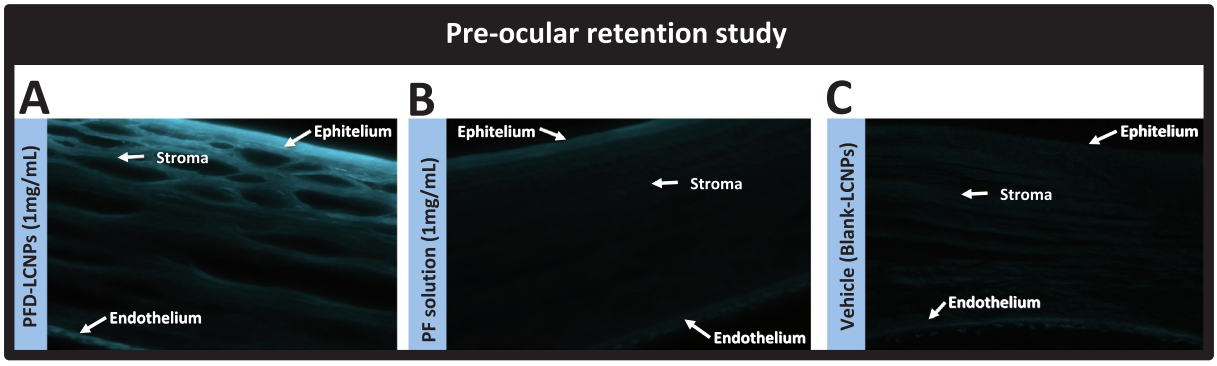

Fig. 9. Pre-ocular retention study showed that PFD-LCNPs promoted a long time of contact of the drug on the corneal surface. (A) PFD-LCNPs at 1 mg/mL, (B) PFD solution at 1 mg/mL, 100 μL and (C) group were treated with vehicle alone (Blank-LCNPs).

tumor necrosis factor-α (TNF-α), monocyte chemoattractant protein-1, interleukin-1β, and interleukin-6, by downregulating the transcription of growth factor-β (TGF-β), and by reducing lipid peroxidation and oxidative stress (Misra and Rabideau, 2000, Oku et al., 2002, Oku et al., 2008). This improvement in the healing pattern of the cornea may thus be related to a reduction of inflammatory cells evidenced by the lower activity of MPO and as demonstrated by histology in the group of animals that were treated with PFD-LCNPs at 1 mg/mL (Fig. 10C).

Although it was described in some studies the presence of macrophages in the inflammatory response in corneal lesions, in this evaluated model of chemical burning there was no difference between groups (Fig. 10B).

4. Conclusion

In summary, the present study demonstrates the potential of a PFD-LCNPs drug delivery system to improve bioavailability. The formulation of PFD-LCNPs was found to be nano-sized, uniformly dispersed, spherical form and exhibited low ocular irritating properties as evaluated by the HET-CAM. Furthermore, the PFD-LCNPs formulation stored in 4 °C presented the best physical stability. The in vitro results showed that PFD-LCNPs were associated with a more sustained release profile than

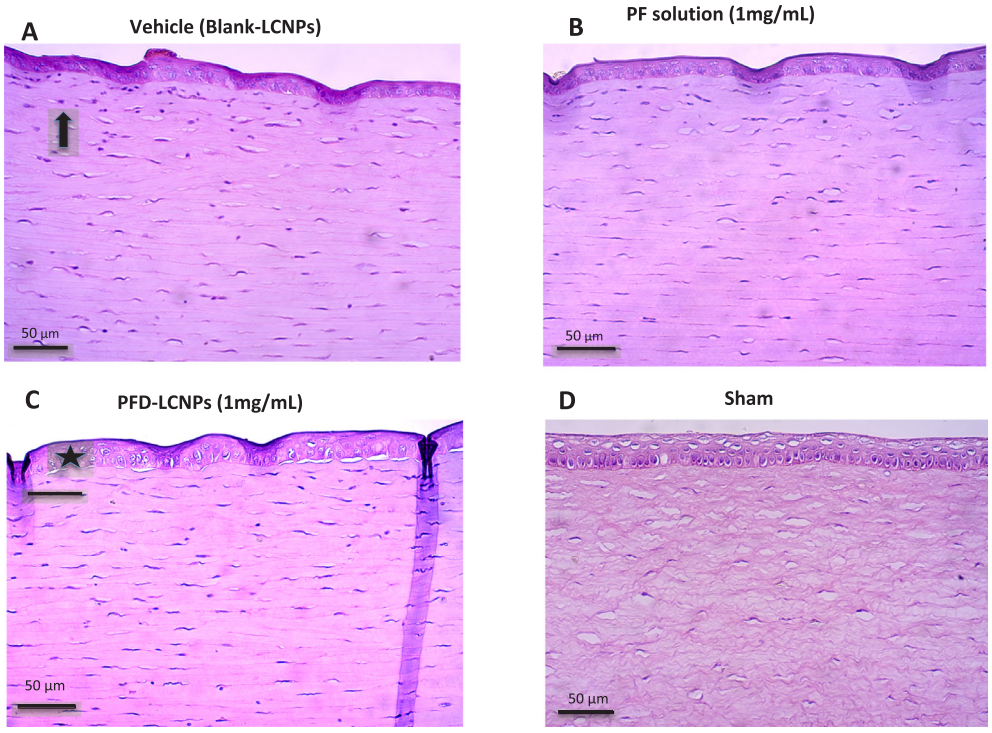

Fig. 10. Histological cross-sections of excised rabbit cornea showing epithelium (EP) and stroma (ST), stained with hematoxylin-eosin after 84 h of injury. (A) group were treated with vehicle alone (Blank-LCNPs), (B) PFD solution at 1 mg/mL, 100 µL and (C) PFD-LCNPs at 1 mg/mL, 100 µL, and (D) Sham. Black arrow indicates inflammatory cells close to the corneal epithelium. Star indicates multilayer epithelial cells.

those achieved using a PFD solution. The *in vivo* evaluation of corneal re-epithelialization time study revealed that PFD-LCNPs at 1 mg/mL exhibited reductions in corneal lesions when compared with the group treated with vehicle (Blank-LCNPs). In addition, histological examination and MPO activity demonstrated the reduction of inflammatory cells when rabbits were treated with PFD-LCNPs. These findings indicated that the biodegradable PFD-LCNPs might have the potential for effective ocular drug delivery.

5. Ethics approval and consent to participate

The study was approved by the commission on ethics on the use of animals of the Federal University of Minas Gerais (CEUA, Belo Horizonte, Brazil, Protocol n° 360/2018). All the experiments were

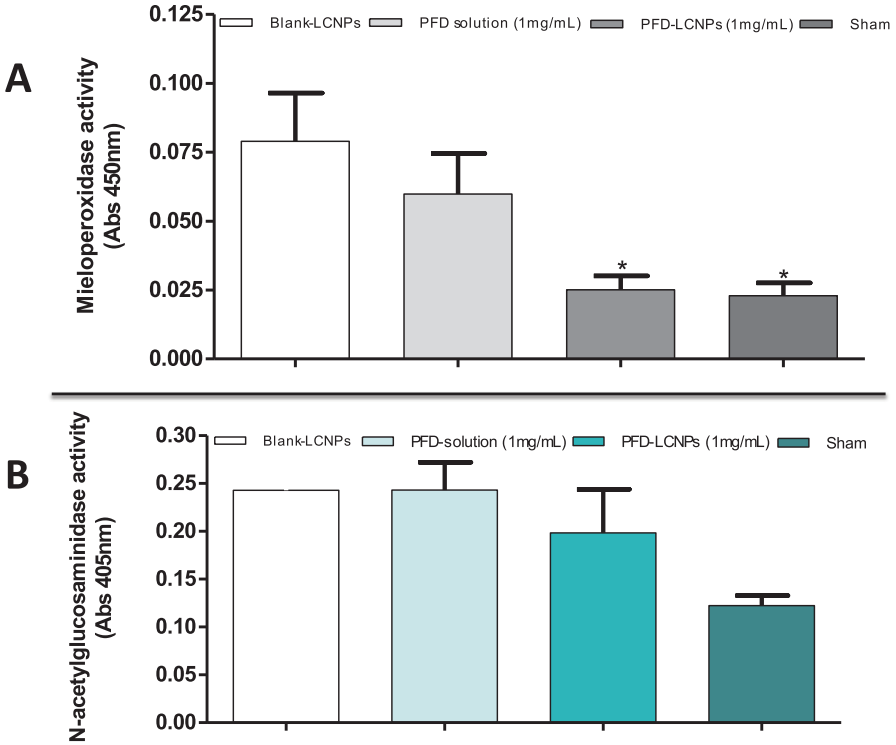

Fig. 11. MPO and NAG measurement. (A) Myeloperoxidase analysis (MPO) of rabbits corneas after 82 h of treatment. (B) N-acetylglucosaminidase activity (NAG) of rabbits corneas after 84 h of treatment. Statistical analyses were performed: *indicates $p < 0.05$ when compared to the vehicle (Blank-LCNPs).

conducted in accordance with the Association for Research in Vision and Ophthalmology (ARVO).

6. Consent for publication

Not applicable.

7. Availability of data and material

The datasets used and/or analyzed during the current study are available from the corresponding author on reasonable request.

Acknowledgments

This work was supported by “Coordenação de Aperfeiçoamento de Pessoal de Nível Superior” (CAPES, Brazil). The authors would like to acknowledge the Center of Microscopy at the Universidade Federal de Minas Gerais (http://www.microscopia.ufmg.br) and Centro de Aquisição e Processamento de Imagens – CAPI at the Universidade Federal de Minas Gerais for providing the equipment and technical support for experiments involving electron microscopy and fluorescence microscopy. This study is part of the National Institute of Science and Technology in Pharmaceutical Nanotechnology, a transdisciplinary approach INCT-NANOFARMA, which is supported by São Paulo Research Foundation (FAPESP, Brazil) Grant #2014/50928-2, by “Conselho Nacional de Desenvolvimento Científico e Tecnológico” (CNPq, Brazil) Grant #465687/2014-8, and by Fundação de Amparo à Pesquisa de Minas Gerais (FAPEMIG, Brazil) Grant #PPM-00456-17.

Declaration of Competing Interests

The authors declare that they have no competing interests.

References

Abdelaziz, H.M., Elzoghby, A.O., Helmy, M.W., Samaha, M.W., Fang, J.Y., Freag, M.S., 2019. Liquid crystalline assembly for potential combinatorial chemo-herbal drug delivery to lung cancer cells. Int. J. Nanomed. 14, 499–517.

Agarwal, R., Iezhitsa, I., Agarwal, P., Abdul Nasir, N.A., Razali, N., Alyautdin, R., Ismail, N.M., 2016. Liposomes in topical ophthalmic drug delivery: an update. Drug Deliv. 23 (4), 1075–1091.

Awwad, S., Mohamed Ahmed, A.H.A., Sharma, G., Heng, J.S., Khaw, P.T., Brocchini, S., Lockwood, A., 2017. Principles of pharmacology in the eye. Br. J. Pharmacol. 174 (23), 4205–4223.

Baradaran-Rafii, A., Eslani, M., Haq, Z., Shirzadeh, E., Huvard, M.J., Djalilian, A.R., 2017. Current and upcoming therapies for ocular surface chemical injuries. Ocul. Surf. 15 (1), 48–64.

Bayhan, Z., Zeren, S., Kocak, F.E., Kocak, C., Akcilar, R., Kargi, E., Tiryaki, C., Yaylak, F., Akcilar, A., 2016. Antiadhesive and anti-inflammatory effects of pirfenidone in postoperative intra-abdominal adhesion in an experimental rat model. J. Surg. Res. 201 (2), 348–355.

Belo, A.V., Barcelos, L.S., Teixeira, M.M., Ferreira, M.A., Andrade, S.P., 2004. Differential effects of antiangiogenic compounds in neovascularization, leukocyte recruitment, VEGF production, and tumor growth in mice. Cancer Invest. 22 (5), 723–729.

Bhattacharjee, S., 2016. DLS and zeta potential – what they are and what they are not? J. Control. Release 235, 337–351.

Borgheti-Cardoso, L.N., Depieri, L.V., Kooijmans, S.A., Diniz, H., Calzzani, R.A., Vicentini, F.T., van der Meel, R., Fantini, M.C., Iyomasa, M.M., Schiffelers, R.M., Bentley, M.V., 2015. An in situ gelling liquid crystalline system based on monoglycerides and polyethylenimine for local delivery of siRNAs. Eur. J. Pharm. Sci. 74, 103–117.

Bruss, M.L., Margolin, S.B., Giri, S.N., 2004. Pharmacokinetics of orally administered pirfenidone in male and female beagles. J. Vet. Pharmacol. Ther. 27 (5), 361–367.

Celia, C., Locatelli, M., Cilurzo, F., Cosco, D., Gentile, E., Scalise, D., Carafa, M., Ventura, C.A., Fleury, M., Tisserand, C., Barbacane, R.C., Fresta, M., Di Marzio, L., Paolino, D., 2015. Long term stability evaluation of prostacyclin released from biomedical device through turbiscan lab expert. Med. Chem. 11 (4), 391–399.

Celia, C., Trapasso, E., Cosco, D., Paolino, D., Fresta, M., 2009. Turbiscan lab expert analysis of the stability of ethosomes and ultradeformable liposomes containing a bilayer fluidizing agent. Colloids Surf. B Biointerfaces 72 (1), 155–160.

Chowdhury, S., Guha, R., Trivedi, R., Kompella, U.B., Konar, A., Hazra, S., 2013. Pirfenidone nanoparticles improve corneal wound healing and prevent scarring following alkali burn. PLoS One 8 (8), e70528.

Danaei, M., Dehghankhold, M., Ataei, S., Hasanzadeh Davarani, F., Javanmard, R., Dokhani, A., Khorasani, S., Mozafari, M.R., 2018. Impact of particle size and polydispersity index on the clinical applications of lipidic nanocarrier systems. Pharmaceutics 10 (2).

Eaton, P., Quaresma, P., Soares, C., Neves, C., de Almeida, M.P., Pereira, E., West, P., 2017. A direct comparison of experimental methods to measure dimensions of synthetic nanoparticles. Ultramicroscopy 182, 179–190.

Esposito, E., Cortesi, R., Drechsler, M., Paccamiccio, L., Mariani, P., Contado, C., Stellin, E., Menegatti, E., Bonina, F., Puglia, C., 2005. Cubosome dispersions as delivery systems for percutaneous administration of indomethacin. Pharm. Res. 22 (12), 2163–2173.

Gaudana, R., Ananthula, H.K., Parenky, A., Mitra, A.K., 2010. Ocular drug delivery. AAPS J. 12 (3), 348–360.

Guo, C., Wang, J., Cao, F., Lee, R.J., Zhai, G., 2010. Lyotropic liquid crystal systems in drug delivery. Drug Discov. Today 15 (23–24), 1032–1040.

Hagerstrom, H., Edsman, K., Stromme, M., 2003. Low-frequency dielectric spectroscopy as a tool for studying the compatibility between pharmaceutical gels and mucous tissue. J. Pharm. Sci. 92 (9), 1869–1881.

Hamill, C.E., Bozorg, S., Peggy Chang, H.Y., Lee, H., Sayegh, R.R., Shukla, A.N., Chodosh, J., 2013. Corneal alkali burns: a review of the literature and proposed protocol for evaluation and treatment. Int. Ophthalmol. Clin. 53 (4), 185–194.

Haring, R.S., Sheffield, I.D., Channa, R., Canner, J.K., Schneider, E.B., 2016. Epidemiologic trends of chemical ocular burns in the United States. JAMA Ophthalmol 134 (10), 1119–1124.

Hughes, P.M., Olejnik, O., Chang-Lin, J.E., Wilson, C.G., 2005. Topical and systemic drug delivery to the posterior segments. Adv. Drug Deliv. Rev. 57 (14), 2010–2032.

Imanishi, J., Kamiyama, K., Iguchi, I., Kita, M., Sotozono, C., Kinoshita, S., 2000. Growth factors: importance in wound healing and maintenance of transparency of the cornea. Prog. Retin Eye Res. 19 (1), 113–129.

Jawaheer, L., Anijeet, D., Ramaesh, K., 2017. Diagnostic criteria for limbal stem cell deficiency-a systematic literature review. Surv. Ophthalmol. 62 (4), 522–532.

Jiang, N., Ma, M., Li, Y., Su, T., Zhou, X.Z., Ye, L., Yuan, Q., Zhu, P., Min, Y., Shi, W., Xu, X., Lv, J., Shao, Y., 2018. The role of pirfenidone in alkali burn rat cornea. Int. Immunopharmacol. 64, 78–85.

Khan, B.F., Harissi-Dagher, M., Khan, D.M., Dohlman, C.H., 2007. Advances in Boston keratoprosthesis: enhancing retention and prevention of infection and inflammation. Int. Ophthalmol. Clin. 47 (2), 61–71.

Khanum, B., Guha, R., Sur, V.P., Nandi, S., Basak, S.K., Konar, A., Hazra, S., 2017. Pirfenidone inhibits post-traumatic proliferative vitreoretinopathy. Eye (Lond.) 31 (9), 1317–1328.

Landau, E.M., Rosenbusch, J.P., 1996. Lipidic cubic phases: a novel concept for the crystallization of membrane proteins. Proc. Natl. Acad. Sci. U.S.A. 93 (25), 14532–14535.

Le, Q., Chen, Y., Wang, X., Li, Y., Hong, J., Xu, J., 2011. Vision-related quality of life in patients with ocular chemical burns. Invest. Ophthalmol. Vis. Sci. 52 (12), 8951–8956.

Lederer, D.J., Bradford, W.Z., Fagan, E.A., Glaspole, I., Glassberg, M.K., Glasscock, K.F., Kardatzke, D., King Jr., T.E., Lancaster, L.H., Nathan, S.D., Pereira, C.A., Sahn, S.A., Swigris, J.J., Noble, P.W., 2015. Sensitivity analyses of the change in FVC in a phase 3 trial of pirfenidone for idiopathic pulmonary fibrosis. Chest 148 (1), 196–201.

Lee, B.S., Margolin, S.B., Nowak, R.A., 1998. Pirfenidone: a novel pharmacological agent that inhibits leiomyoma cell proliferation and collagen production. J. Clin. Endocrinol. Metab. 83 (1), 219–223.

Lee, J., Kellaway, I.W., 2000. Buccal permeation of [D-Ala(2), D-Leu(5)]enkephalin from liquid crystalline phases of glyceryl monooleate. Int. J. Pharm. 195 (1–2), 35–38.

Li, J., Wu, L., Wu, W., Wang, B., Wang, Z., Xin, H., Xu, Q., 2013. A potential carrier based on liquid crystal nanoparticles for ophthalmic delivery of pilocarpine nitrate. Int. J. Pharm. 455 (1–2), 75–84.

Liang, L., Li, W., Ling, S., Sheha, H., Qiu, W., Li, C., Liu, Z., 2009. Amniotic membrane extraction solution for ocular chemical burns. Clin. Exp. Ophthalmol. 37 (9), 855–863.

Lin, X., Yu, M., Wu, K., Yuan, H., Zhong, H., 2009. Effects of pirfenidone on proliferation, migration, and collagen contraction of human Tenon’s fibroblasts in vitro. Invest. Ophthalmol. Vis. Sci. 50 (8), 3763–3770.

Liu, R., Wang, S., Fang, S., Wang, J., Chen, J., Huang, X., He, X., Liu, C., 2016. Liquid crystalline nanoparticles as an ophthalmic delivery system for tetrandrine: development, characterization, and in vitro and in vivo evaluation. Nanoscale Res. Lett. 11 (1), 254.

Macias-Barragan, J., Sandoval-Rodriguez, A., Navarro-Partida, J., Armendariz-Borunda, J., 2010. The multifaceted role of pirfenidone and its novel targets. Fibrogenesis Tissue Repair 3, 16.

Manaia, E.B., Abucafy, M.P., Chiari-Andreo, B.G., Silva, B.L., Oshiro Junior, J.A., Chiavacci, L.A., 2017. Physicochemical characterization of drug nanocarriers. Int. J. Nanomed. 12, 4991–5011.

McCormick, S., Nelson, A., Nauseef, W.M., 2012. Proconvertase proteolytic processing of an enzymatically active myeloperoxidase precursor. Arch. Biochem. Biophys. 527 (1), 31–36.

Mencucci, R., Favuzza, E., Boccalini, C., Lapucci, A., Felici, R., Resta, F., Chiarugi, A., Cavone, L., 2014. CoQ10-containing eye drops prevent UVB-induced cornea cell damage and increase cornea wound healing by preserving mitochondrial function. Invest. Ophthalmol. Vis. Sci. 55, 7266–7271.

Mishraki, T., Ottaviani, M.F., Shames, A.I., Aserin, A., Garti, N., 2011. Structural effects of insulin-loading into HII mesophases monitored by electron paramagnetic resonance (EPR), small angle X-ray spectroscopy (SAXS), and attenuated total reflection Fourier transform spectroscopy (ATR-FTIR). J. Phys. Chem. B 115 (25), 8054–8062.

Misra, H.P., Rabideau, C., 2000. Pirfenidone inhibits NADPH-dependent microsomal lipid peroxidation and scavenges hydroxyl radicals. Mol. Cell. Biochem. 204 (1–2), 119–126.

Nagarwal, R.C., Kant, S., Singh, P.N., Maiti, P., Pandit, J.K., 2009. Polymeric

nanoparticulate system: a potential approach for ocular drug delivery. J. Control. Release 136 (1), 2–13.
Okada, Y., Shirai, K., Miyajima, M., Reinach, P.S., Yamanaka, O., Sumioka, T., Kokado, M., Tomoyose, K., Saika, S., 2016. Loss of TRPV4 function suppresses inflammatory fibrosis induced by alkali-burning mouse corneas. PLoS One 11 (12), e0167200.
Oku, H., Nakazato, H., Horikawa, T., Tsuruta, Y., Suzuki, R., 2002. Pirfenidone suppresses tumor necrosis factor-alpha, enhances interleukin-10 and protects mice from endotoxic shock. Eur. J. Pharmacol. 446 (1–3), 167–176.
Oku, H., Shimizu, T., Kawabata, T., Nagira, M., Hikita, I., Ueyama, A., Matsushima, S., Torii, M., Arimura, A., 2008. Antifibrotic action of pirfenidone and prednisolone: different effects on pulmonary cytokines and growth factors in bleomycin-induced murine pulmonary fibrosis. Eur. J. Pharmacol. 590 (1–3), 400–408.
Pahuja, P., Arora, S., Pawar, P., 2012. Ocular drug delivery system: a reference to natural polymers. Expert Opin. Drug Deliv. 9 (7), 837–861.
Patel, V.R., Agrawal, Y.K., 2011. Nanosuspension: an approach to enhance solubility of drugs. J. Adv. Pharm. Technol. Res. 2 (2), 81–87.
Rezvani, M., Hesari, J., Peighambardoust, S.H., Manconi, M., Hamishehkar, H., 2018. Development and characterization of nanostructured pharmacosomal mesophases: an innovative delivery system for bioactive peptides. Adv. Pharm. Bull. 8 (4), 609–615.
Rodrigues, L., Kyriakos, K., Schneider, F., Dietz, H., Winter, G., Papadakis, C.M., Hubert, M., 2016. Characterization of lipid-based hexosomes as versatile vaccine carriers. Mol. Pharm. 13 (11), 3945–3954.
Rossetti, F.C., Fantini, M.C., Carollo, A.R., Tedesco, A.C., Bentley, M.V., 2011. Analysis of liquid crystalline nanoparticles by small angle X-ray diffraction: evaluation of drug and pharmaceutical additives influence on the internal structure. J. Pharm. Sci. 100 (7), 2849–2857.
Semeraro, F., Forbice, E., Braga, O., Bova, A., Di Salvatore, A., Azzolini, C., 2014. Evaluation of the efficacy of 50% autologous serum eye drops in different ocular surface pathologies. Biomed. Res. Int. 2014, 826970.
Shah, J.C., Sadhale, Y., Chilukuri, D.M., 2001. Cubic phase gels as drug delivery systems. Adv. Drug Deliv. Rev. 47 (2–3), 229–250.
Shanbhag, S.S., Saeed, H.N., Paschalis, E.I., Chodosh, J., 2018. Boston keratoprosthesis type 1 for limbal stem cell deficiency after severe chemical corneal injury: a systematic review. Ocul. Surf. 16 (3), 272–281.
Sharma, N., Singh, D., Maharana, P.K., Kriplani, A., Velpandian, T., Pandey, R.M., Vajpayee, R.B., 2016. Comparison of amniotic membrane transplantation and umbilical cord serum in acute ocular chemical burns: a randomized controlled trial. Am. J. Ophthalmol. 168, 157–163.
Shi, S., Wu, J., Chen, H., Chen, H., Wu, J., Zeng, F., 2007. Single- and multiple-dose pharmacokinetics of pirfenidone, an antifibrotic agent, in healthy Chinese volunteers. J. Clin. Pharmacol. 47 (10), 1268–1276.
Silva, C.N.D., Silva, F.R.D., Dourado, L.F.N., Reis, P., Silva, R.O., Costa, B.L.D., Nunes, P.S., Amaral, F.A., Santos, V.L.D., de Lima, M.E., Silva Cunha Junior, A.D., 2019. A new topical eye drop containing LyeTxI-b, a synthetic peptide designed from A Lycosa erithrognata venom toxin, was effective to treat resistant bacterial keratitis. Toxins (Basel) 11 (4).
Stepp, M.A., Zieske, J.D., Trinkaus-Randall, V., Kyne, B.M., Pal-Ghosh, S., Tadvalkar, G., Pajoohesh-Ganji, A., 2014. Wounding the cornea to learn how it heals. Exp. Eye Res. 121, 178–193.
Sun, G., Lin, X., Zhong, H., Yang, Y., Qiu, X., Ye, C., Wu, K., Yu, M., 2011. Pharmacokinetics of pirfenidone after topical administration in rabbit eye. Mol. Vis. 17, 2191–2196.
Tamilvanan, S., Benita, S., 2004. The potential of lipid emulsion for ocular delivery of lipophilic drugs. Eur. J. Pharm. Biopharm. 58 (2), 357–368.
Trivedi, R., Redente, E.F., Thakur, A., Riches, D.W., Kompella, U.B., 2012. Local delivery of biodegradable pirfenidone nanoparticles ameliorates bleomycin-induced pulmonary fibrosis in mice. Nanotechnology 23 (50), 505101.
Trujillo-Cayado, L.A., Ramirez, P., Alfaro, M.C., Ruiz, M., Munoz, J., 2014. Adsorption at the biocompatible alpha-pinene-water interface and emulsifying properties of two eco-friendly surfactants. Colloids Surf. B Biointerfaces 122, 623–629.
Vandamme, T.F., 2002. Microemulsions as ocular drug delivery systems: recent developments and future challenges. Prog. Retin. Eye Res. 21 (1), 15–34.
Vandoolaeghe, P., Barauskas, J., Johnsson, M., Tiberg, F., Nylander, T., 2009. Interaction between lamellar (vesicles) and nonlamellar lipid liquid-crystalline nanoparticles as studied by time-resolved small-angle X-ray diffraction. Langmuir 25 (7), 3999–4008.
Verma, P., Ahuja, M., 2016. Cubic liquid crystalline nanoparticles: optimization and evaluation for ocular delivery of tropicamide. Drug Deliv. 23 (8), 3043–3054.
Wagoner, M.D., 1997. Chemical injuries of the eye: current concepts in pathophysiology and therapy. Surv. Ophthalmol. 41 (4), 275–313.
Warren, M., Atkinson, K., Steer, S., 1990. INVITTOX: the ERGATT/FRAME data bank of in vitro techniques in toxicology. Toxicol. In Vitro 4 (4–5), 707–710.
Wisniewska, M., Chibowski, S., Urban, T., Sternik, D., Terpilowski, K., 2016. Impact of anionic polyacrylamide on stability and surface properties of the Al2O3–polymer solution system at different temperatures. Colloid Polym. Sci. 294 (9), 1511–1517.
Yamagami, K., Oka, T., Wang, Q., Ishizu, T., Lee, J.K., Miwa, K., Akazawa, H., Naito, A.T., Sakata, Y., Komuro, I., 2015. Pirfenidone exhibits cardioprotective effects by regulating myocardial fibrosis and vascular permeability in pressure-overloaded hearts. Am. J. Physiol. Heart Circ. Physiol. 309 (3), H512–522.